ISSN 0469-4732

INSTITUTE OF PLASMA PHYSICS

NAGOYA UNIVERSITY

Full Consistent Analysis of High Beta Steady State Tokamaks Sustained by Beam Driven and Bootstrap Currents

K. Okano, Y. Ogawa and H. Naitou

(Received — May 18, 1989)

IPPJ-912 May 1989

RESEARCH REPORT

NAGOYA, JAPAN

FULL CONSISTENT ANALYSIS OF HIGH BETA STEADY STATE TOKAMAKS SUSTAINED BY BEAM DRIVEN AND BOOTSTRAP CURRENTS

K. OKANO*, Y. OGAWA and H. NAITOU+

(Received - May 18, 1989)

IPPJ-912 May 1989

Further communication about this report is to be sent to the Research Information Center, Institute of Plasma Physics, Nagoya University, Nagoya 464-01, Japan

---

+ Present address: Yamaguchi Univ., Faculty of Engineering

* Permanent address: TOSHIBA Research and Development Center, 4-1, Ukishima-cho, Kawasaki 210, Japan.

ABSTRACT

Beam driven steady state tokamaks of moderate size (R_o = 4.55 m) is analyzed by a full consistent beam current drive analysis code, which consistently includes MHD equilibrium, kink and ballooning stability analysis, bootstrap current, power balance and momentum balance calculations. It was found that this moderate size is sufficient to demonstrate the feasibility of steady state operation by the neutral beam current drive. The maximum Q value attains $Q = 7 \sim 9$ with the fusion power $P_f = 500 \sim 800$ MW and L-mode confinement is sufficient to sustain self consistent equilibria. The Q value is nearly doubled due to the bootstrap current and the $T_i > T_e$ feature of beam driven tokamaks. The optimum beam energy is $1.0 \sim 1.2$ MeV and the toroidal rotation effects has been negligible.

1. INTRODUCTION

MHD stability analysis is indispensable in a high beta steady state tokamak study, because the plasma current and its profile play essential roles for determining stability. The plasma current profile and its drive power must be decided so as to satisfy the MHD stability condition. The authors reported in a previous paper (Okano et al., 1989a) the development of a beam current drive code DRIVER which gives a solution consistent with the 2-D MHD equilibrium analysis by EQLAUS (Gruber et al., 1981a) and the kink and ballooning mode stability analysis by ERATO (Gruber et al., 1981b; Naitou et al., 1988). This code has been upgraded to DRIVER-88 and includes a self-consistent power balance analysis and a bootstrap current calculation. The fast ion Fokker-Planck code has also been replaced by the bounce-averaged type. Therefore, the new code fully includes the toroidal effect on the fast ion current as well as on the beam induced electron current. The beam deposition is calculated by a three dimensional model, which includes the exact calculation of beam stopping cross-section enhancement due to multi-step ionization (MSI) (Boley et al., 1984).

The outline of the study using this new code was presented previously (Okano et al., 1989b). This paper gives a report on it in more detail with new toroidal field scans and plasma rotation study.

In our previous study (1989a), where the bootstrap current and the MSI beam stopping cross-section enhancement were not included, we concluded that the maximum energy

gain Q (≈ fusion power P_f/beam power P_b) for next generation tokamaks would be less than 5 if the conventional Dee type plasma cross-section is used, and the optimum beam energy, for maximizing the Q value, was 600∿800 keV. In the present paper, it is shown that inclusion of bootstrap current and the MSI effect highly improves the Q value. A moderate size tokamak (R_o = 4.55 m, Dee type, P_f = 500∿800 MW) was assumed in this study, then the Q value, optimized with L-mode confinement, attained up to 8.4, which is sufficient for demonstration tokamak reactors. The optimum beam energy also increases up to 1.0∿1.2 MeV. Although this paper concentrates on discussing about such next generation tokamaks, the results suggest that Q>> 20 would be achievable for larger power reactors where P_f is several gigawatts, because Q is improved by an increase in P_f, as shown in the above paper.

2. CURRENT DRIVE ANALYSIS IN CRITICAL BETA EQUILIBRIA

2.1 Outline

Many parameter scans were made for a moderate size tokamak with critical beta equilibria determined by the kink and ballooning mode analysis. The standard parameters used here are: [R_0 = 4.55 m, a = 1.66 m, elongation κ = 1.8 (Dee), I_t = 19.6 MA, B_t = 4.7 T, β_t = 6.05 %]. The values of I_t and B_t were changed in the B_t scan cases. Since the machine size effect was already studied in our previous paper (1989a), the plasma size was not scanned in this study. The critical beta MHD equilibrium for this configuration is shown in Fig. 1 and Table 1. Its details were described in the previous papers (Naitou et al., 1988 and Okano et al., 1989a). In this equilibrium, the current and pressure profiles have been nearly optimized and the beta value has been maximized as high as possible in this plasma configuration. The optimization manner was described in the above papers. The safety factor q_ψ on the plasma surface has been reduced down to 2.05 in order to maximize the toroidal beta value $\bar{\beta}_t$. The central value of q_ψ is 1.15. Although $\bar{\beta}_t$ attains 6.05 %, the ERATO code showed that the kink, Mercier and ballooning modes are still stable without conductive shell. Troyon ratio g [= $\bar{\beta}_t/(I_t/aB_t)$] is 2.40, which seems to be comparably low [for example, the reference value in the ITER design is $g = 2.9$ with $q_\psi = 3$]. But, this is a conventional feature for any low q_ψ (< 3) equilibria, where the $\bar{\beta}_t$ value is mainly restricted by the kink mode instability.

The beam current drive analysis code system (DRIVER-88) is composed of a 3-D beam power & toroidal momentum deposition code and a 2-D Fokker-Planck code. The details were described in the previous papers (Okano et al., 1988 and 1989a), except that, in the present code, the bounce averaged type has been used for the Fokker-Planck code, and MSI beam stopping cross-section enhancement is included in the beam deposition code.

The power profile in the beam line, $P_{inj}(Z)$, can be taken into account [Fig. 2]. This power profile is controlled automatically to reproduce the current profile required by the MHD analysis. The minimum major radius of the beam center line is expressed by R_{tang}. In this study, R_{tang} = 4.8 m ($\sim$ magnetic axis R_x) has been assumed, except for R_{tang} scan cases. This R_{tang} choice gives the maximum Q value (see §4.3). The beam line has a rectangular cross-section of 0.5 m width and ±2.5 m symmetrical height. Beam energy E_b was set to 1 MeV, except for its scan case. As shown in §4.4, this beam energy also gives the maximum Q value. The beam tilting angle θ_v was set to zero in this study. The beam divergence was also set to zero, because it is usually very small for a high energy beam system.

2.2 MSI Cross Section Enhancement

The beam stopping cross-section enhancement due to the multi-step collision process was studied by Boley et al. (1984). The cross-section with/without the enhancement is calculated by the numerical database supplied to the authors by C. Boley and D. Post. In this study, the iron impurity and a 5 % helium concentration were assumed. Since the enhancement data for the helium ion is not available at present, we have assumed that the enhancement rate for helium ions is the same as that for hydrogen ions. The error due to this approximation is considered to be negligible, because low Z ion contributions to δ are usually small.

The cross-section enhancement rate $1 + \delta$ is very sensitive to the plasma parameters, especially to density as well as to beam energy. Therefore, δ must be local values in the plasma. In the DRIVER code, the enhancement rates are calculated for the individual ionization events along the beam line. The $1 + \delta$ value is about unity near the plasma periphery and $1 + \delta > 1.5$ near the plasma center, because δ strongly depends on the density; the MSI effect is highly overestimated if a constant δ value is used instead of its local values, as pointed out previously (Okano and Ogawa, 1988).

2.3 Beam Driven and Bootstrap Currents

The beam driven current density $\langle j_b \rangle_k$ between the flux surfaces labeled by the flux functions ψ_{k-1} and ψ_k is given by

$$\langle j_b \rangle_k = \langle j_i \rangle_k \left[1 - \frac{Z_b}{Z_{eff}} \{1 - G(Z_{eff}, \varepsilon_k)\}\right] , \qquad (1)$$

where the flux surface average fast ion current $\langle j_i \rangle_k$ is evaluated by the Fokker-Planck calculation, and Z_{eff} is the effective charge of plasma, Z_b is the beam ion charge number and ε_k is the inverse aspect ratio of the flux surface labeled by ψ_k. The factor G expresses the toroidal effect on the beam induced back streaming electron currents (Start et al., 1980).

The bounce averaged Fokker-Planck equations were solved on the 100 individual flux surfaces, using the eigenfunctions for the model operator given by Cordey (1976). The ion current densities were evaluated numerically by the arbitrary aspect ratio model without the small ε_k limit approximation, which was used in the above reference.

The bootstrap current density was evaluated by the model of Hirshman (1978). The model includes the contributions of all thermal species and the impurity effects, but the effect of supra-thermal ions (like alpha particles) was neglected.

The relationship between the MHD equilibrium current density and the r.f. driven current density was studied by

Ehst (1985). The application of his model to the beam driven current was described in our paper (Okano et al., 1989a); the beam driven current density $\langle j_b \rangle$ must satisfy the following relationship:

$$\langle j_b \rangle = \frac{\langle j \cdot B \rangle}{\langle B^2 \rangle} \langle B \rangle - \frac{\langle j_{bs} \cdot B \rangle}{\langle B^2 \rangle} \langle B \rangle \quad ,$$

where $\langle\ \rangle$ means the flux surface average $\langle F \rangle = \int F B_p^{-1} d\ell / \int B_p^{-1} d\ell$, j and j_{bs} are the MHD equilibrium and bootstrap current densities, respectively, and $\langle j_b \rangle$ is identical to the value given by Eq. (1). The convergence algorithm to satisfy the above relationship is described in Section 3.2.

3. SELF-CONSISTENT ANALYSIS WITH MHD AND POWER BALANCE CODES

3.1 Power and Momentum Balances

The authors suggested that the temperature ratio $\bar{T}_i/\bar{T}_e$ could be larger than unity in beam driven tokamaks and that this high $\bar{T}_i$ feature would enhance the Q value (Okano et al., 1989a). In this study, a dual component (elec. & ion) 0-D power balance code was used to investigate the above problem. This code includes the coronal equilibrium calculation for radiation cooling rates and mean charge states for various impurities (Post et al., 1977); the charge states of ions depend on the electron temperatures, but the Z_{eff} value was kept constant at its specified value by automatic adjustment of the iron impurity concentration.

The power balance equations are given by

$$Q_i/\tau_{Ei} = P_{fi} + P_{bi} - P_{ie} \qquad (2)$$

$$Q_e/\tau_{Ee} = P_{fe} + P_{be} + P_{ie} + P_{oh} - P_{rad} \qquad (3)$$

where $Q_i(Q_e)$ are the ion (electron) total energies, $P_{fi}(P_{fe})$ and $P_{bi}(P_{be})$ are the alpha and beam heating terms, P_{ie} is the ion-electron energy relaxation term, and P_{rad} is the total radiation power. The ohmic power P_{oh} was set to zero. The ion energy confinement time τ_{Ei} has been assumed as to be 1/3 of the neo-classical value. This τ_{Ei} choice, however, is not so important, because the $\bar{T}_i$ value is rather dominated by the ion-electron energy relaxation in the considered parameter range. On the other hand, the electron energy confinement time τ_{Ee} is very ambiguous in the

present database, and its impact on the electron temperature is not small. Therefore, $\bar{T}_e$ was given as an input value in this study instead of introducing an ambiguous τ_{Ee} model, thus τ_{Ee} and the global energy confinement time τ_E were calculated backwards and compared with the L-mode confinement scaling τ_{KG} (Kaye, 1985). The density weighted average temperature $\bar{T}_j$ is defined as

$$\bar{T}_j = \int n_j T_j dV / \int n_j dV \quad . \tag{4}$$

Using $\bar{T}_j$, the total energy of species j is written as $Q_j = (3/2)\bar{n}_j \bar{T}_j V_p$, where V_p is the plasma volume.

The 0-D toroidal momentum balance equation is given by

$$R_o R_\phi / \tau_\phi = \sum_j m_j R_o \int n_j v_\phi dV \quad , \tag{5}$$

where τ_ϕ is the toroidal momentum confinement time, v_ϕ is the local toroidal rotation speed, m_j is the mass of species j, and R_ϕ is the total momentum input. The spatial profile of v_ϕ was assumed to be similar to the ion temperature profile, as observed in TFTR (Scott et al., 1988). The effects of the local rotation speed have been taken into account in the calculations of the beam deposition, driven current, beam pressure and beam direct reaction power P_{TCT}. Three options can be chosen for the rotation effect calculation: (1) τ_ϕ is given, (2) $\tau_\phi = C_\phi \tau_E$ with a constant C_ϕ, (3) the average rotation speed $\langle v_\phi \rangle$ is given,

where $\langle v_\phi \rangle = \sum \int n_j m_j v_\phi dV / \sum \int n_j m_j dV$. In this study, we used the first option with $\tau_\phi = 2 \sim 3$ sec. This value was $2 \sim 3$ times τ_E in the present case, and this is not inconsistent with the recent TFTR experiments.

The evaluation of v_ϕ is very ambiguous, because there is no reliable scaling formula for τ_ϕ to date. Therefore, the cases with no rotation are mainly discussed in this paper. The rotation effects are taken into account only in the case of rotation effect study in §4.4. However, the rotation effects on the current drive efficiency and on the energy gain Q were usually small.

3.2 Full Consistent Analysis Algorithm

The authors' full consistent code has been constructed according to the reverse solution algorithm (Okano et al., 1989a). First, a critical beta equilibrium is determined by EQLAUS/ERATO iterative calculations, where the current j_ψ and the pressure p_ψ are optimized. Next, the driven current profile and the total pressure profile converge to these critical beta profiles [$\langle j \cdot B \rangle B / \langle B^2 \rangle$ and p_{total} in Fig. 1] by optimizing the thermal pressure profile and the beam power distribution $P_{inj}(z)$ in the beam line, denoted in Fig. 2. The driven current includes the bootstrap current, and the total pressure is composed of thermal, beam ion and fast alpha pressures. The thermal pressure profile is adjusted by changing the density profiles, while the temperature profiles are maintained during the iteration. The beam deposition, current profile control, pressure adjustment, power balance and momentum balance calculation processes are iterated about 30 times, and usually all parameters and these profiles converge within 2 % accuracy. The final converged solution is consistent with the critical beta equilibrium given by EQLAUS/ERATO, and gives optimized $P_{inj}(z)$ and density profiles. At the same time, $\bar{T}_i$, τ_{Ee}, τ_E and $\langle v_\phi \rangle$ converge to self consistent values in the present new code. An example of converged solutions is shown in Fig. 1, where the same parameters as in Fig. 6-c were used.

The conventional algorithm of self-consistent current drive analysis with MHD equilibria was developed by Ehst

et al. for r.f. driven current (Ehst, 1985 / Ehst, Evans and Ignat, 1986). The simular algorithm was also used for the beam driven current (Okano, Shinya et al., 1986 / Yamamoto, Okano et al., 1987 / Devoto, 1988). In this conventional algorithm, the current driver parameters are given first, and the MHD equilibrium sustained by the non-inductive current is determined by MHD/current drive iterative calculations. In such a method, the final solution is usually inconsistent with the critical beta conditions in the current and pressure profiles. In the recent papers on the r.f. current drive by Hsiao, Ehst et al. (1989) and by Ehst and Evans (1989), this probelm is fairly improved by controlling the current profile with idealized r.f. wave parameters. In the beam driven current analysis, however, the pressure profile is largely modified by the current profile control, because of the existence of beam pressure. This fact highly complicates the self-consistent analysis of beam driven tokamaks. In our algorithm, the current and pressure profiles are controlled simultaneously. In contrast with the conventional method, the current driver parameters, to sustain the pre-optimized MHD equilibrium, is obtained in the final solution; this is the reason for naming the 'reverse solution'.

The solutions always converge to the same pre-optimized MHD equilibrium in the reverse solution algorithm. Since the bootstrap current is very sensitive to the q_ψ profile, this feature of reverse solution code is a very important

merit in the present parametric study; pure parameter dependencies of bootstrap current contribution can be studied, while insulating from its q_ψ dependence.

4. PARAMETRIC SCANS

4.1 Electron Temperature and Bootstrap Current

The $\bar{T}_e$ value was scanned from 16 keV to 26 keV with the temperature profile $T(\psi) \propto 1 - s^4$, where s is the ratio of the width of the flux surface labeled by ψ and the plasma width 2a. The results are summarized in Fig. 3. The solid lines and broken lines are for the $Z_{eff} = 1.5$ case and $Z_{eff} = 2.0$ case, respectively. As shown in Fig. 3-c, $\bar{T}_i$ is much larger than $\bar{T}_e$. The beam power P_b decreases with $\bar{T}_e$ [Fig. 3-e], but the fusion output P_f also decreases [Fig. 3-b], because the density is changed in the reverse solution code to maintain the total pressure. Thus, the Q values have maxima at $\bar{T}_e \sim 18$ keV with $P_b \sim 70$ MW ($Z_{eff} = 1.5$) and at $\bar{T}_e \sim 22$ keV with $P_b \sim 65$ MW ($Z_{eff} = 2.0$) [Fig. 3-a]. It is worth noting that both maxima of Q (~ 9) correspond to $\bar{T}_i \sim 30$ keV. This fact suggests that the maxima of Q is conditioned by $\bar{T}_i$ (~ 30 keV) rather than by $\bar{T}_e$.

The Q-values for the $\bar{T}_i = \bar{T}_e$ case, where the power balance was switched off, are also plotted in Fig. 3-a and b (dotted lines). It is clarified that the above high $\bar{T}_i$ feature of beam driven tokamaks enhances the Q-value. Note that this enhancement rate is reduced with $\bar{T}_e$ increment, and the Q value attains the same value as in the $\bar{T}_e \neq \bar{T}_i$ cases at $\bar{T}_i = \bar{T}_e \sim 26$ keV. The maximum in Q for $\bar{T}_i = \bar{T}_e$ case occurs at $\bar{T}_i \sim 30$ keV again, while $\bar{T}_e > 26$ keV is not shown in the figure.

The τ_E value, normalized by the Kaye-Goldston L-mode

value τ_{KG} (Kaye, 1985) is plotted in Fig. 3-f. The L-mode confinement, given by K-G scaling, seems to be sufficient to sustain these equilibria. With τ_E of 0.9 ∿ 1.3 times τ_{KG}, the Q-value, $7 < Q < 9$, can be expected. The requirement on τ_E is reduced in the steady state tokamaks because the power close to alpha heating is continuously injected by the current driver.

In the conventional L-mode discharges on which the L-mode τ_E scaling is based, $\bar{T}_e \sim \bar{T}_i$ and the electron energy loss is the main loss channel, and thus $\tau_E \sim \tau_{Ee}$ is expected. In the high T_i mode, the global energy confinement may be improved (Zarnstorff et al., 1989). And we might compare τ_{KG} with τ_{Ee}, rather than with τ_E, in our $T_i >> T_e$ cases. In our EPS paper (Okano et al., 1989b), τ_{Ee}/τ_{KG} was plotted for the present results instead of τ_E/τ_{KG}. In this case, the situation was more optimistic. Lower P_b operations were expectable with higher $\bar{T}_e$ under $\tau_{Ee} = \tau_{KG}$ conditions.

The bootstrap (BS) current ratio I_{bs}/I_t is about 35 % ∿ 40 % [Fig. 3-d], where I_t is the total current. The dependence on $\bar{T}_e$ is comparably weak. The bootstrap current contributes to Q enhancement in two ways. The first is, of course, the direct reduction of the beam power. The second is indirect. The beam power reduction results in a lower beam pressure. Thus, the fuel ion pressure (and fusion power) increases and the Q value is enhanced under constant beta conditions. Therefore, the Q enhancement rate by the BS current is usually larger than I_{bs}/I_t.

The change in P_f and Q due to the BS current are compared in Fig. 4. The Q improvement by the BS current is about 40 %. The Q enhancement rate $1 - Q_o/Q_{bs}$ is shown in Fig. 4-c with I_{bs}/I_t, where Q_{bs} and Q_o are the Q values with the without BS current, respectively. The $1 - Q_o/Q_{bs}$ value is larger than I_{bs}/I_t at $\bar{T}_e > 18$ keV because of the P_f increment. In the $\bar{T}_e < 18$ keV range, this P_f increment effect on Q is nearly cancelled by the current drive efficiency deterioration due to the fuel density increment.

L-mode operation parameters, where $\tau_E = \tau_{KG}$, are listed in Table 2 for two cases: $Z_{eff} = 1.5$ and 2.0.

The lower Z_{eff} results in a lower $\bar{T}_e$ but leads to a higher $\bar{T}_i$ and a larger P_f. Therefore, the Q value is improved in the $Z_{eff} = 1.5$ case. The bootstrap current contributions are nearly the same in both cases (38 % and 37 %). However, the I_{bs}/I_t ratio is sensitive to the temperature profile (see the next section). A broad temperature profile has been assumed here, which is desirable to enhance the bootstrap current. The beam shinethrough fraction f_s is the same and moderate in both cases (5.8 %).

4.2 Temperature Profile Effects on Q and BS Current

In the present algorithm, a different temperature profile choice leads to another solution with a different density profile. T_e and T_i profiles were given by $T \propto 1 - s^{\alpha_1}$. The T-profile scan results are summarized in Figs. 5 and 6, where α_1 was changed from 2 (parabolic) to 6 (broad) and $\bar{T}_e$ = 18 keV. A peaked temperature profile results in a broad density profile and vice versa. The authors had found that the Q value was somewhat larger for a broader T-profile due to fusion power increment, in no BS current case (1989a). The present results show that I_{bs}/I_t is also larger for a broader T-profile (Fig. 5, and j_{bs} profiles are shown in Fig. 6). The Q value increases from 6 (at α_1 = 2) to 10 (at α_1 = 6), and P_b decreases from 104 MW to 79 MW. However, the changes in $\bar{T}_i$, in the current drive efficiency $\gamma = (n_e/10^{20}) \cdot R \cdot I_b/P_{abs}$ and in the shinethrough fraction f_s are all very small, where I_b is the beam driven current ($I_b = I_t - I_{bs}$) and $P_{abs} = (1 - f_s)P_b$. The required $P_{inj}(z)$ profiles depend strongly on the T-profiles (Fig. 6). For $\alpha_1 \geq 4$, a main central beam (beam height = ±1 m with a Gaussian P_{inj} profile) seems to be sufficient to drive the seed current, with an additional small edge control beam (at $z \sim \pm 2$ m).

During the present temperature profile scans, the authors excluded any hollow profile case, because of its ambiguity in achievement. If the hollow temperature profiles are acceptable, the I_{bs}/I_t value may be highly enhanced

up to 100 % (Ané et al., 1989). However, such a large bootstrap current contribution will also be restricted by the MHD stability condition in the current profile.

4.3 Beam Line Orientation; R_{tang}

In the previous study without MSI cross-section enhancement, the range $R_o - a/2 < R_{tang} < R_o - a/4$ was desirable to minimize the beam shinethrough fraction f_s. However, in the new calculation including the MSI enhacement, the f_s minimum point appears near $R_{tang} \sim R_o$ as shown in Fig. 7-a, where $\bar{T}_e$ = 18 keV and E_b = 1 MeV. A small R_{tang} and a reduced beam penetration by MSI cause current drive efficiency deterioration due to trapped ion orbits, especially near the plasma periphery. Therefore, power injected near the periphery should be increased to maintain the current profile. This, in turn, promotes beam shinethrough through the low density edge. Therefore, the f_s minimum point shifts toward a larger R_{tang}.

The case without MSI is shown in Fig. 7-b. The difference in $P_{inj}(z)$ between MSI ON and OFF becomes considerable near the periphery. The shinethrough power is localized near the edge, and the f_s is doubled without MSI enhancement. The γ value is slightly larger in the MSI OFF case, but this γ improvement is nearly cancelled by the f_s increment; the Q value is nearly the same in both cases. In the uniform plasma, the shinethrough f_s is proportional to $\exp(-\sigma)$, where σ is the ionization cross-section. Therefore, it is convenient to define the effective cross-section enhancement rate $[1 + \delta]_{eff}$ in the non-uniform plasma as;

$$[1 + \delta]_{eff} = \ell n\, f_s^{ON} / \ell n\, f_s^{OFF} \quad , \qquad (6)$$

where f_s^{ON} and f_s^{OFF} are the f_s values with and without MSI effect, respectively. The $[1+\delta]_{eff}$ value is in the $1.2 \sim 1.3$ range in the present case, as shown in Fig. 7-a. It is worth noting that, if an average value of $1+\delta$ is estimated by $\bar{n}_e$ and $\bar{T}_e$, it exceeds 1.5, and leads to an underestimation of the f_s value. The three dimensional calculation is very essential in the estimation of MSI effects.

Although f_s is minimized at $R_{tang} \sim R_o$, the Q value is maximized at a larger R_{tang} ($\sim R_x$), where R_x is the magnetic axis major radius. Therefore, R_{tang} = 4.8 m ($\sim R_x$) has been chosen as the standard value in this study. R_{tang} value larger than 'R_x + half beam width' is not available, since the current profile becomes hollow intrinsically.

4.4 Beam Energy and Toroidal Rotation

Increasing E_b ($\lesssim$ 2 MeV) improves the γ value. But it enhances the shinethrough, and reduces P_{TCT} (= the fusion power due to beam direct reactions), as shown in Fig. 8, where $\bar{T}_e$ = 18 keV. Moreover, $\bar{T}_i$ decreases with E_b, because a larger beam power goes to electrons with a higher E_b. As a result, the Q value is maximized at E_b = 1.0 $\sim$ 1.2 MeV with Q $\sim$ 9. This Q value is twice as large as the no BS current case without power balance analysis (Okano et al., 1989a) and the optimum E_b has been increased to 1 MeV from 600 keV due to the MSI cross-section enhancement. However, it is worth noting that the Q deterioration, by decreasing E_b down to 600 keV from 1 MeV, is only 17 %, and Q is still high enough ($\sim$ 7.5). Also note that such a low E_b operation leads to a very high T_i mode ($\bar{T}_i$ = 37 keV for $\bar{T}_e$ = 18 keV).

The toroidal rotation effects on Q and γ are plotted in Fig. 9, where three cases, τ_ϕ = 0, 2 and 3 seconds, have been considered. The average rotation velocity $\langle v_\phi \rangle$ is less than 10^6 m/s and decreases with E_b increment because the input power and momentum are lower for a higher E_b. The impact on γ is very small for E_b > 1 MeV. The impact on Q is also small, and surprisingly, Q rather increases slightly at E_b > 1 MeV. This is because P_{TCT} increases with $\langle v_\phi \rangle$ increment. It should be remembered that P_{TCT}/P_b decreases with the effective beam energy increment in the over 200 keV range (Jassby, 1977). Nevertheless, the change in Q is minor over the considered energy range even when

τ_ϕ = 3 sec ($\sim$ 3 τ_E).

The beam energy optimization studies to date for next generation tokamaks are summarized in Table 3. Since the databases on the MSI and toroidal rotation effects are insufficient, the ambiguous range of optimum beam energy is 0.6 MeV to 1.4 MeV. An advisable target for beam development seems to be in the 0.8 $\sim$ 1.0 MeV range.

4.5 B_t, Fusion Power and Confinement Improvement

Since the MHD stability is analyzed in normalized MHD equilibria, B_t scan, while keeping critical beta equilibria, is possible if j_ψ/B_t and p_ψ/B_t^2 are maintained, where B_t is the toroidal field at $R = R_o$. The results of B_t scan are summarized in Fig. 10, where B_t = 4.5, 4.6, 4.7 and 4.8 T, respectively, and accordingly, I_t = 18.8, 19.2, 19.6 and 20.0 MA. (The standard values in other parts of this paper are B_t = 4.7 T and I_t = 19.6 MA.) A higher B_t leads to a larger output power P_f, and thus, results in an improvement in the Q value. Since a higher $\bar{T}_e$ leads to a lower P_f, the Q value is not improved. In any case, Q saturates at $Q \sim 9$ with B_t = 4.8 T. However, this Q saturation can be overcome by increasing the machine size with the output power. Such machine size effects were studied in the previous paper (Okano et al., 1989a).

The confinement improvement from τ_{KC} makes a higher $\bar{T}_e$ operation possible, as shown Fig. 10-a. However, as described above, a higher $\bar{T}_e$ operation does not improve the Q value. Nevertheless, it is worth noting that, if τ_E is improved up to 1.4 τ_{KG}, the required beam power (= P_f/Q) is reduced down to 53 MW, with B_t = 4.7 T, P_f = 460 MW, Q = 8.6 and $\bar{T}_e$ = 22 keV. This beam power is nearly half the power in Table 2, while P_f is also halved. It is reported from many recent tokamak experiments that the L-mode confinements are improved by 20 $\sim$ 40 % with peaked density profiles and/or high $\bar{T}_i/\bar{T}_e$ ratios (Zarnstoff et al. 1989 / Nagami

et al., 1989 / Bhatnagar et al., 1989 / Kaufmann et al., 1989 / Mori et al., 1989), which are just the cases.

5. Summary and Conclusions

The ion temperature $\bar{T}_i$ is much larger than $\bar{T}_e$ in beam driven tokamaks. This high $\bar{T}_i$ feature improves the Q value about 20 % ∿ 30 %. The bootstrap current attains 20 ∿ 40 % in the total driven currents and improves the Q value accordingly. The MSI cross-section enhancement also contributes to the Q enhancement, because the beam orientation can be optimized with an acceptable shinethrough. The Q value is doubled by these three effects and is maximized at $E_b \sim 1$ MeV. Although a moderate size tokamak (R_o = 4.55 m, Dee type, B_t = 4.7 T, I_t = 19.6 MA) was assumed with L-mode confinement, the attainable Q value is 7 to 9, which seems to be sufficient for next generation tokamaks and is close to the requirement in the ITER design with R_o = 5.7 m.

The optimum beam energy to maximize the Q value is 1.0 MeV ∿ 1.2 MeV. Further increment in E_b does not lead to any Q enhancement, but causes a lower output power and a heavy shinethrough. Decreasing E_b down to 600 keV leads to a very high T_i mode ($\bar{T}_i$ = 37 keV with $\bar{T}_e$ = 18 keV), and the Q deterioration is less than 20 %. The Q reduction due to toroidal rotation is minor over the considered E_b range ($E_b \geqq 0.6$ MeV).

The confinement improvement does not increase the Q value but makes a considerable beam power reduction possible. For example, 40 % τ_E improvement results in 50 % beam power saving.

The moderate size (R_o = 4.55 m) tokamak proposed here

would not satisfy the ohmic burning condition. However, a steady state operation with $Q = 7 \sim 9$ is achievable by 1 MeV beam injection. Such a middle size steady state machine would be one of the clever choices to demonstrate the feasibility of steady state tokamaks.

Acknowledgments

The authors would like to acknowledge Drs. C. Boley and D. Post for providing the MSI database. Dr. A. Hatayama is also thanked for his efforts in power balance code development. The comments by Dr. F. Umibe were very valuable to improve the manuscript. This work was carried out on the computer at the Institute of Plasma Physics of Nagoya University under its collaborative research programme.

References

Ané J. M., Laurent L., Samain A. (1989), Proc. 16th Europ. Conf. on Contr. Fusion and Plasma Phys., Venice, Vol. 4, P. 1323.

Bhatnagar V. P., Taroni A., Ellis, J. J., Jacquinot J., Start D. F. H. (1989), ibid, Vol. 1, P. 127.

Boley C. D., Janev R. K., Post D. E. (1984), Phys. Rev. Lett. 52, P. 534.

Cordey J. G. (1976), Nucl. Fusion 16, P. 499.

Devoto R. S. (1988), in ITER Current Drive and Heating Workshop, Garching.

Ehst D. A. (1985), Nucl. Fusion 25, P. 629.

Ehst D. A., Evans K. Jr., Ignat D. W. (1986), Nucl. Fusion 26, P. 461.

Ehst D. A., Evans K. Jr. (1989), 'Maximal Bootstrap Current Tokamak Equilibria in the First Stability Regime', Argonne National Laboratory Report, ANL/FPP/TM-235, Argonne, USA.

Gruber R., Troyon F., Berger D., Bernard L. C., Rousset S., Schreiber R., Kerner W., Schneider W., Roberts K. W. (1981a), Comput. Phys. Commun. 21, P. 323.

Gruber R., Semenzato S., Troyon F., Tsunematsu T., Kerner W., Merkel P., Schneider W. (1981b), Comput. Phys. Commun. 24, P. 363.

Hirshmann S. P. (1978), Phys. Fluids 21, P. 1295.

Hsiao M.-Y., Ehst D. A., Evans K. Jr. (1989), Nucl. Fusion 29, P. 49.

Jassby D. L. (1977), Nucl. Fusion 17, P. 309.

Kaufmann M. et al. (1989), Proc. 16th Europ. Conf. on Contr. Fusion and Plasma Phys., Venice, Vol. 1, P. 47.

Kaye S. M. (1985), Phys. Fluids 28, P. 2327.

Mikkelsen D. R., Singer C. E. (1983), Nucl. Technol./Fusion 4, P. 237.

Mori M. et al. (1989), Proc. 16th Europ. Conf. on Contr. Fusion and Plasma Phys., Venice, Vol. 1, P. 213.

Naitou H., Yamazaki K. (1988), Nucl. Fusion 28, P. 1715.

Nagami M. and JT-60 Team (1989), 'Recent Results in JT-60 Experiments', invited paper in 16th Europ. Conf. on Contr. Fusion and Plasma Phys., Venice, to be published in Plasma Phys. Contr. Fusion.

Okano K., Shinya K., Yamato H. (1986), in US-JAPAN Workshop on Non-Circular Tokamaks, San Diego.

Okano K., Yamamoto S., Sugihara M., Fujisawa N. (1988), 'Potential of Neutral Beam Current Drive for Steady State and Quasi-Steady State Tokamak Reactors', accepted for publication by Fusion Technology: Preprint, JAERI-M 87-209, Japan Atomic Energy Research Institute, Japan (1988).

Okano K., Ogawa Y. (1988), 'NBCD for a Critical Beta Plasma', in ITER Current Drive and Heating Workshop, Garching.

Okano K., Ogawa Y., Naitou H. (1989a), Nucl. Fusion 29, P. 199.

Okano K., Ogawa Y., Naitou H. (1989b), Proc. 16th Europ. Conf. on Contr. Fusion and Plasma Phys., Venice, Vol. 4, P. 1307.

Post D. E., Jensen R. V. (1977), Atomic Data and Nuclear Data Tables 20, P. 397.

Scott S. D. et al. (1988), 'Current Drive and Confinement of Angular Momentum in TFTR', in IAEA Int. Conf. on Plasma Phys. and Contr. Nucl. Fusion Res., Nice, IAEA-CN-50/E-3-5.

Start D. F. H., Cordey J. G. (1980), Phys. Fluids 23, P. 1477.

Yamamoto S., Okano K., Nishio S., Sugihara M. et al. (1987), Proc. 11th IAEA Int. Conf. on Plasma Phys. and Contr. Nucl. Fusion Res., Vol. 3, P. 267, IAEA, Vienna.

Zarnstorff M. C., Goldston R. J. et al. (1989), Proc. 16th Europ. Conf. on Contr. Fusion and Plasma Phys., Venice, Vol. 1, P. 35.

Captions

Table 1 Critical beta plasma parameters, determined by kink and ballooning mode analysis.

Table 2 Consistent parameters with τ_{KG} scaling.

Table 3 Summary of beam energy optimization studies for next generation tokamaks.

Fig. 1 Example of full consistent solutions, where the same parameters as in Fig. 6-c were used ($\bar{T}_e$ = 18 keV, E_b = 1 MeV).

Fig. 2 Schematic drawing of beam line in the calculations.

Fig. 3 Summary of $\bar{T}_e$ scans, where E_b = 1 MeV and R_{tang} = 4.8 m. Z_{eff} = 2.0 for $\bar{T}_e = \bar{T}_i$ case.

Fig. 4 Q enhancement due to bootstrap current.

Fig. 5 Temperature profile effects, where $T \propto 1 - s^{\alpha_1}$ $\bar{T}_e$ = 18 keV, E_b = 1 MeV and R_{tang} = 4.8 m.

Fig. 6 $P_{inj}(z)$ and bootstrap current profiles.

Fig. 7 Optimization of beam line orientation and MSI effects, where $\bar{T}_e$ = 18 keV, E_b = 1 MeV and α_1 = 4.

Fig. 8 Summary of beam energy scans, where $\bar{T}_e$ = 18 keV, α_1 = 4 and R_{tang} = 4.8 m.

Fig. 9 Toroidal rotation impacts on Q and $\Upsilon = \bar{n}_e R_o I_b / (1 - f_s) \cdot P_b$, where $\bar{T}_e$ = 18 keV, α_1 = 4, R_{tang} = 4.8 m and $v_\phi(s) \propto T_i(s)$.

Fig. 10 Summary of B_t scans, where E_b = 1 MeV, R_{tang} = 4.8 m, τ_ϕ = 0, and α_1 = 4. I_t = 19.6 (MA)$\cdot(B_t/4.7$ T).

Table 1 Critical beta plasma parameters, determined by kink and ballooning mode analysis.

Major radius	R_0	4.55 m
Plasma width	a	1.66 m
Plasma volume	V_p	436 m^3
Aspect ratio	A	2.75
Plasma elongation	κ	1.80
Plasma triangularity	δ	0.30
Toroidal beta	$\bar{\beta}_t$	6.05 %
Poloidal beta	$\bar{\beta}_p$	0.486
Plasma current	I_t	$0.915 R_0 B_{to}$ (MA)
q_ψ (surface/center)		2.05/1.15
$g = \bar{\beta}_t/(I_t/aB_{to})$ [Troyon ratio]		2.40

Table 2 Consistent parameters with τ_{KG} scaling

Z_{eff}	1.5	2.0
$\bar{T}_e$/keV*	16.8	18.0
$\bar{T}_i$/keV*	25.5	24.0
$\bar{n}_e/m^{-3}$	0.59×10^{20}	0.60×10^{20}
P_f/MW	840	800
P_b/MW	100	104
Q	8.4	7.7
I_{bs}/I_t	38 %	37 %
f_s	5.8 %	5.8 %
τ_E/sec	0.94	0.97

* $\bar{T}_j = \int n_j T_j dV / \int n_j dV$

Table 3. SUMMARY OF BEAM ENERGY OPTIMIZATION STUDIES FOR NEXT GENERATION TOKAMAKS

2-D F-P Equation	○	○	○	○	○
3-D Beam Deposition	—	○	○	○	○
Beam-Plasma DT-Reaction	—	○	○	○	○
MHD Analysis	—	—	○	○	○
Bounce-Averaged F-P	—	—	—	○	○
Power Balance	—	—	—	○	○
Multi-Step Ionization	—	—	—	○	○
Toroidal Rotation	—	—	—	—	○
Beam Energy For Max Q	1.5∿2.0 MeV	1.0∿1.5 MeV	0.6∿0.8 MeV	1.0∿1.2 MeV	1.0∿1.4 MeV
References	(*)	Okano et al. (1988)	← (1989a)	← (1989b)	this study

(*) For example, Mikkelsen and Singer (1983).

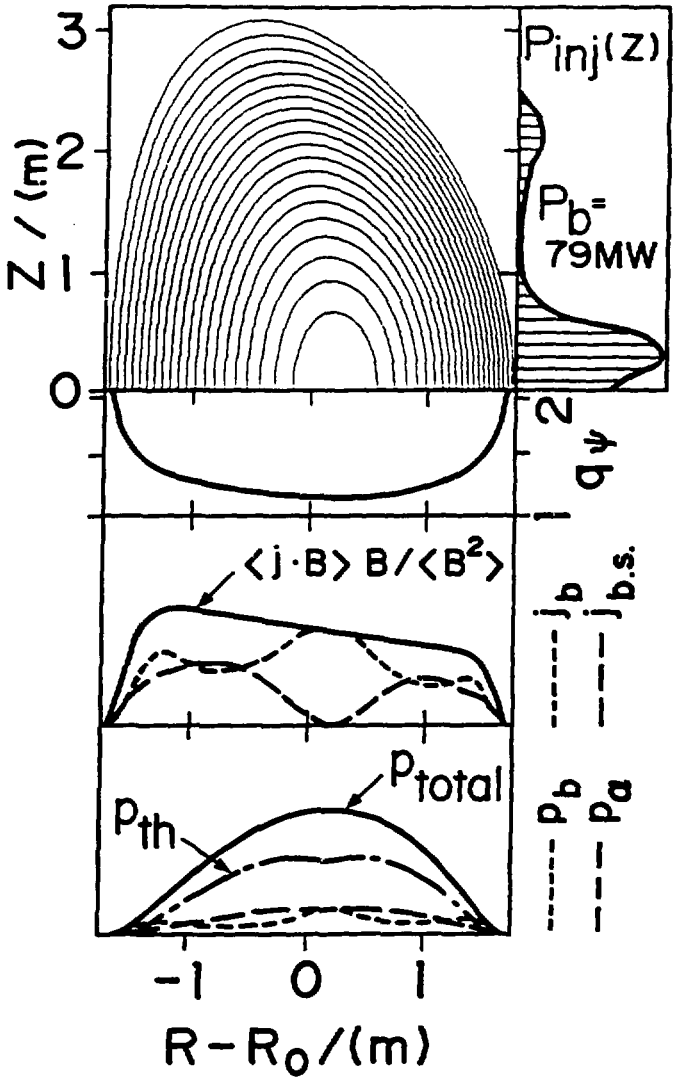
3
2
1
0
Z / (m)
Pinj(Z)
Pb=
79MW
2
qψ
1
<j·B> B/<B²>
jb
jb.s.
ptotal
pth
pb
pa
-1
0
1
R-R0/(m)

Fig. 1

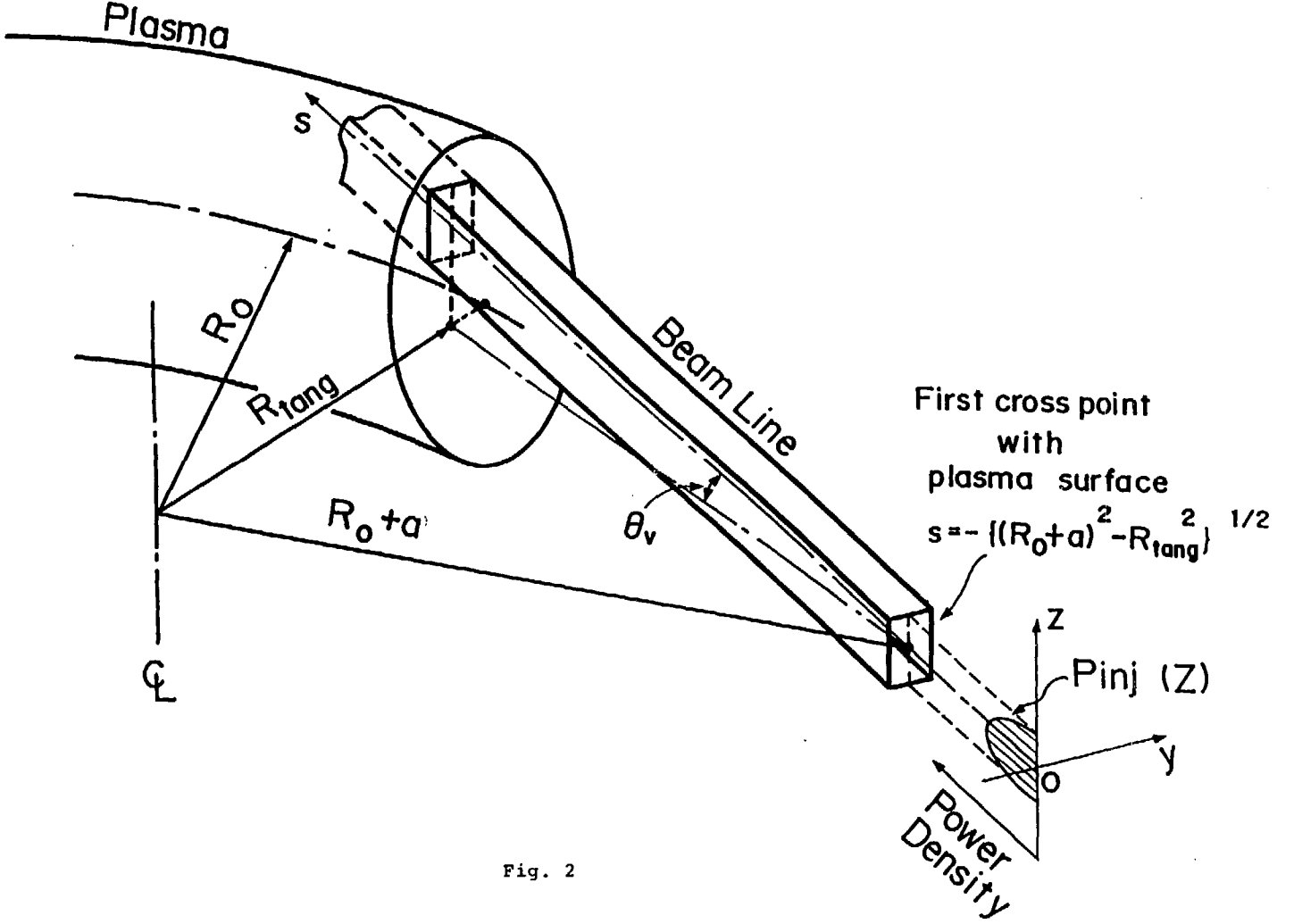
Plasma
s
R_o
R_{tang}
R_o+a
θ_v
Beam Line
First cross point
with
plasma surface
$s=-\{(R_o+a)^2-R_{tang}^2\}^{1/2}$
z
Pinj (Z)
y
o
Power
Density
℄

Fig. 2

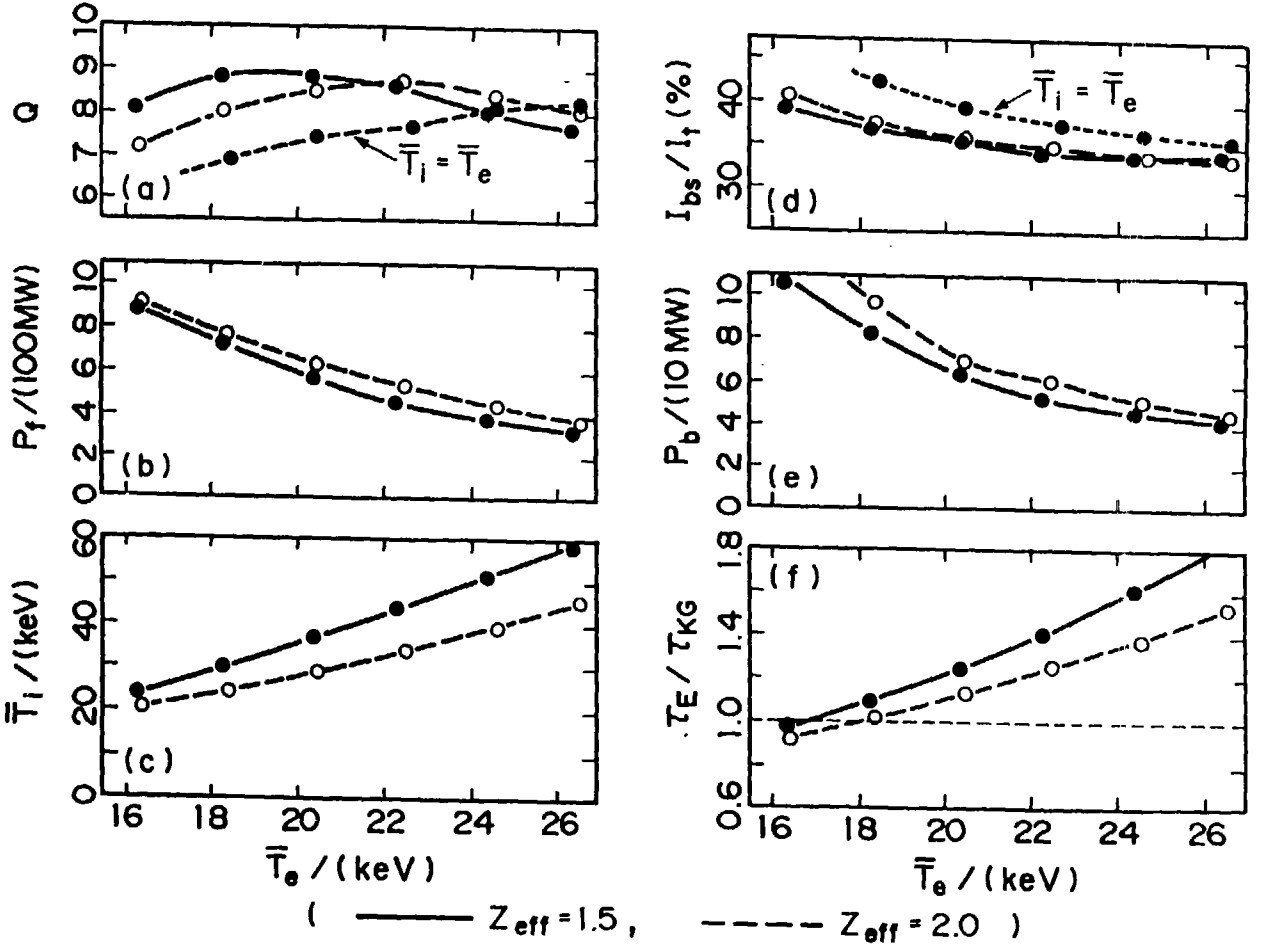
Q
(a)
$\bar{T}_i = \bar{T}_e$
P_f/(100MW)
(b)
$\bar{T}_i$/(keV)
(c)
$\bar{T}_e$/(keV)
I_{bs}/I_t(%)
(d)
$\bar{T}_i = \bar{T}_e$
P_b/(10MW)
(e)
τ_E/τ_{KG}
(f)
$\bar{T}_e$/(keV)
(——— Z_{eff}=1.5, ---- Z_{eff}=2.0)

Fig. 3

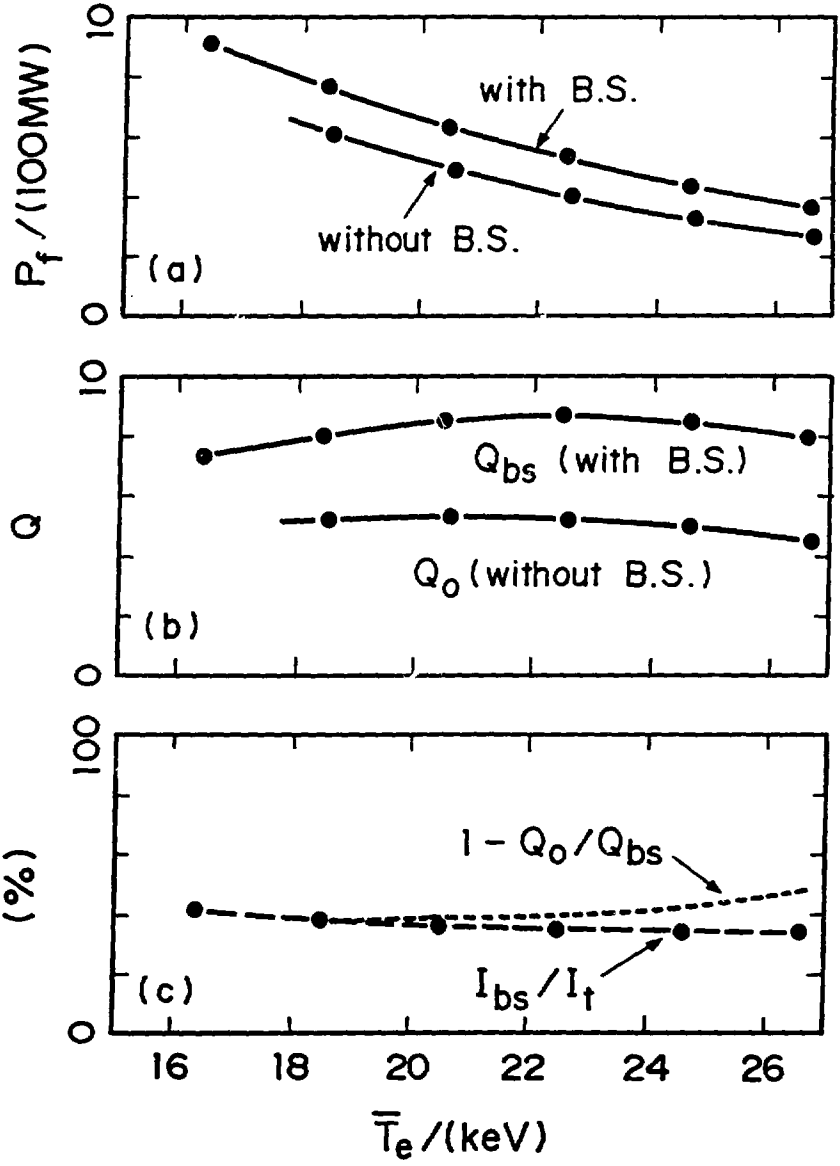
10
0
P_f/(100MW)
with B.S.
without B.S.
(a)
10
0
Q
Q_{bs} (with B.S.)
Q_o (without B.S.)
(b)
100
0
(%)
$1 - Q_o/Q_{bs}$
I_{bs}/I_t
(c)
16
18
20
22
24
26
$\bar{T}_e$/(keV)

Fig. 4

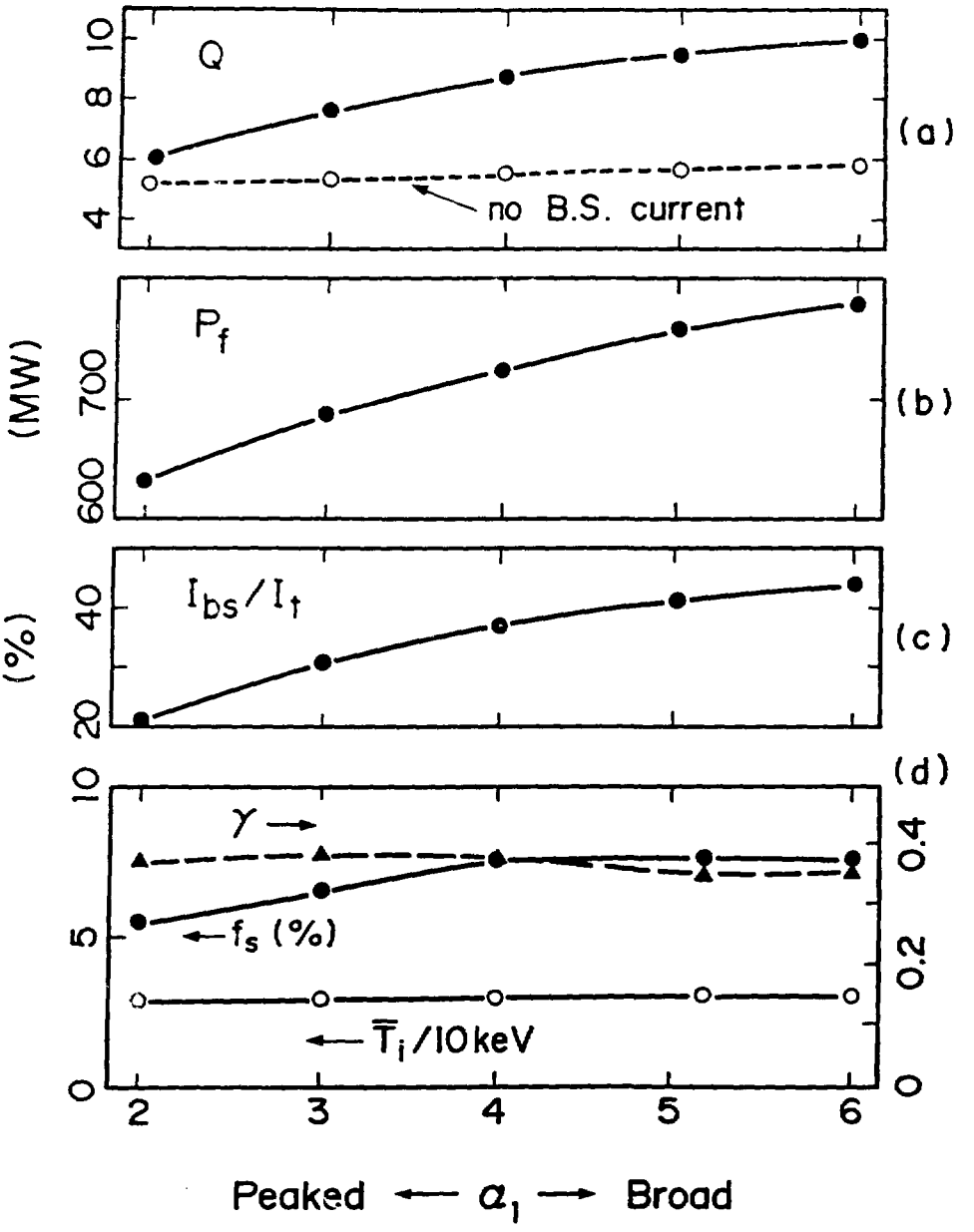
Q
(a)
no B.S. current
P_f
(MW)
(b)
I_{bs}/I_t
(%)
(c)
(d)
γ
f_s (%)
$\bar{T}_i$/10keV
Peaked ← α_1 → Broad

Fig. 5

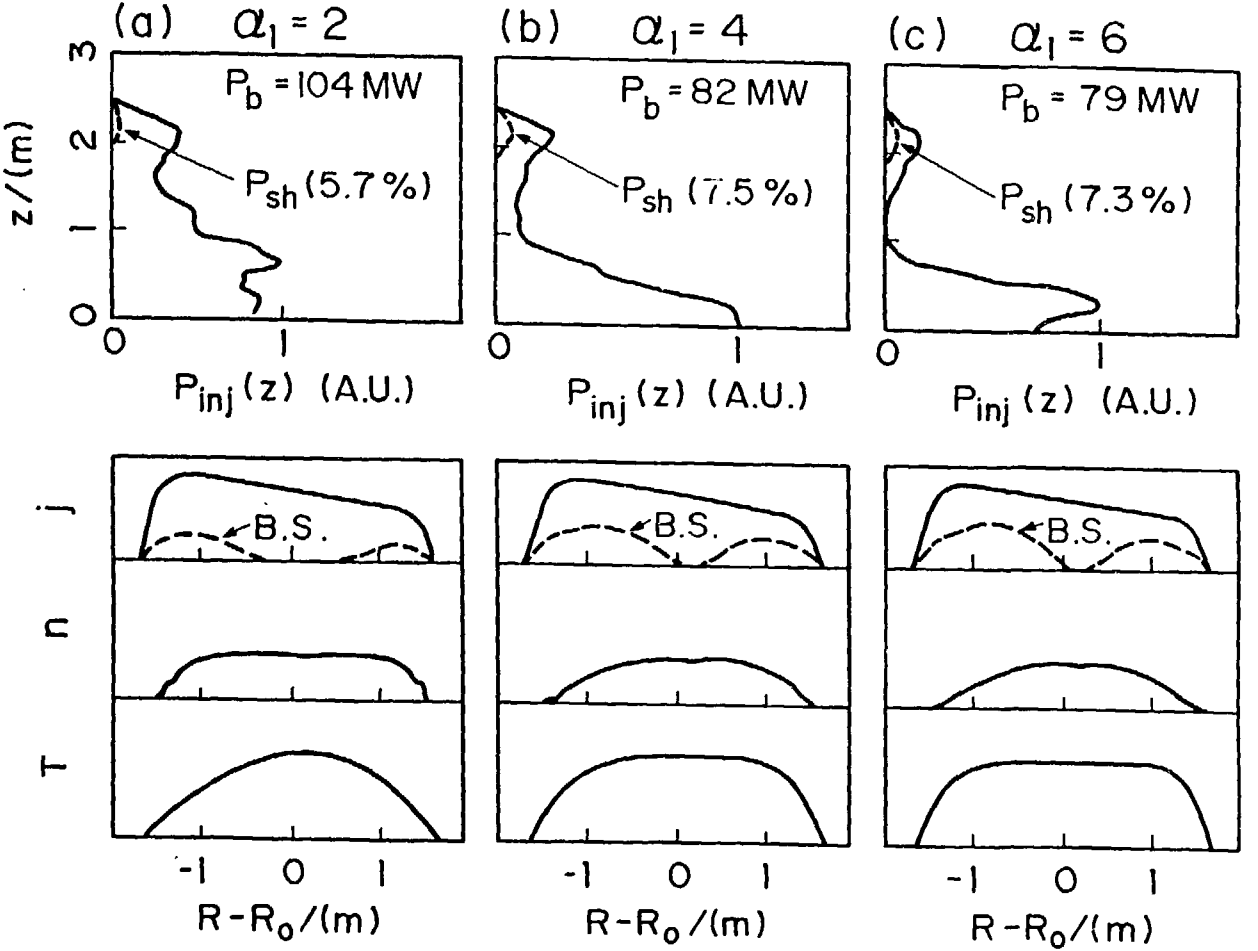
(a) $\alpha_1 = 2$
(b) $\alpha_1 = 4$
(c) $\alpha_1 = 6$
P_b = 104 MW
P_b = 82 MW
P_b = 79 MW
P_{sh} (5.7 %)
P_{sh} (7.5 %)
P_{sh} (7.3 %)
z/(m)
P_{inj} (z) (A.U.)
B.S.
n j
T
R - R_0 /(m)

Fig. 6

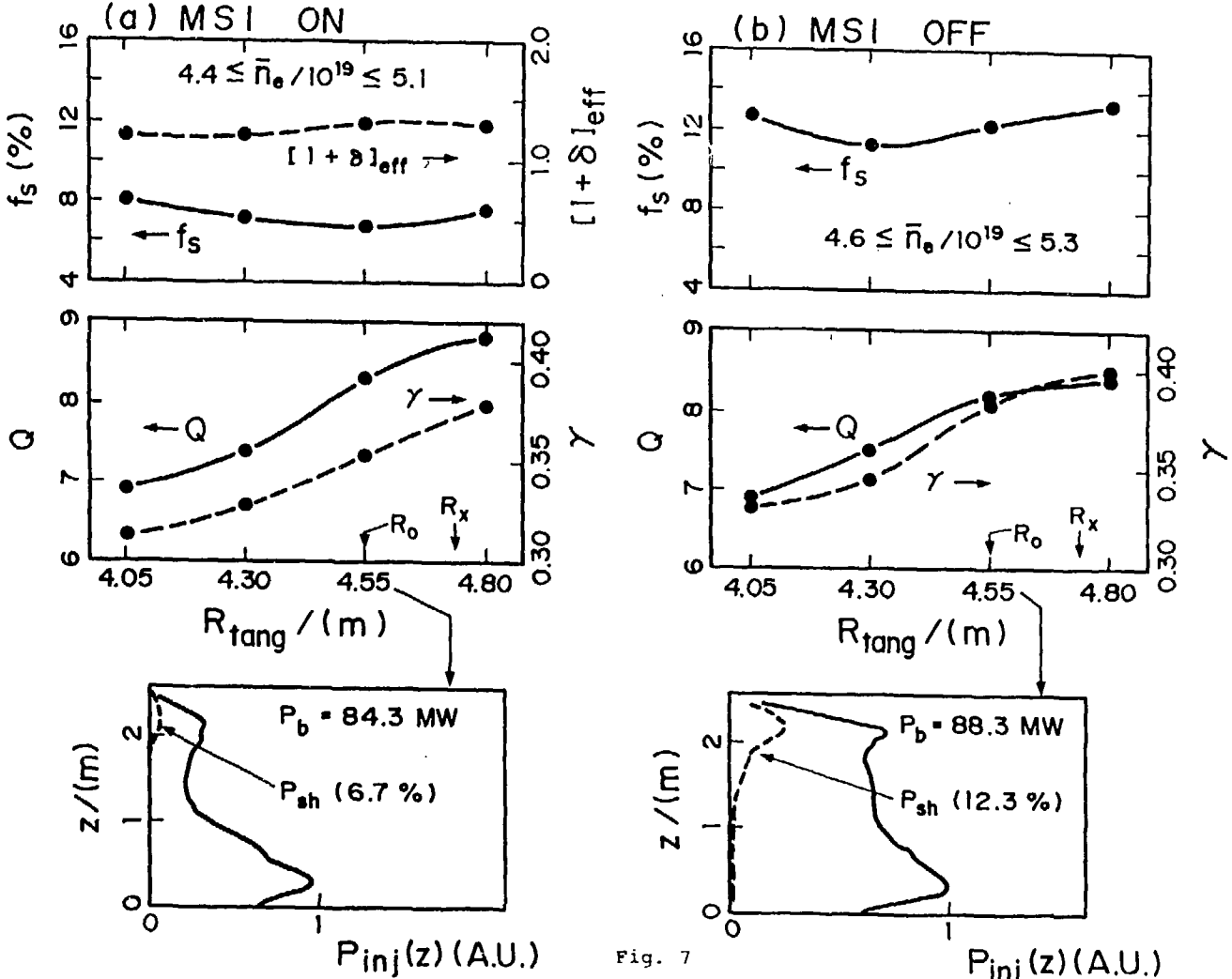
(a) MSI ON
4.4 ≤ n̄e /10^19 ≤ 5.1
[1 + δ]eff
fs
fs (%)
[1+δ]eff
Q
γ
Ro
Rx
4.05
4.30
4.55
4.80
Rtang /(m)
Pb = 84.3 MW
Psh (6.7 %)
z /(m)
Pinj(z) (A.U.)
(b) MSI OFF
4.6 ≤ n̄e /10^19 ≤ 5.3
Pb = 88.3 MW
Psh (12.3 %)

Fig. 7

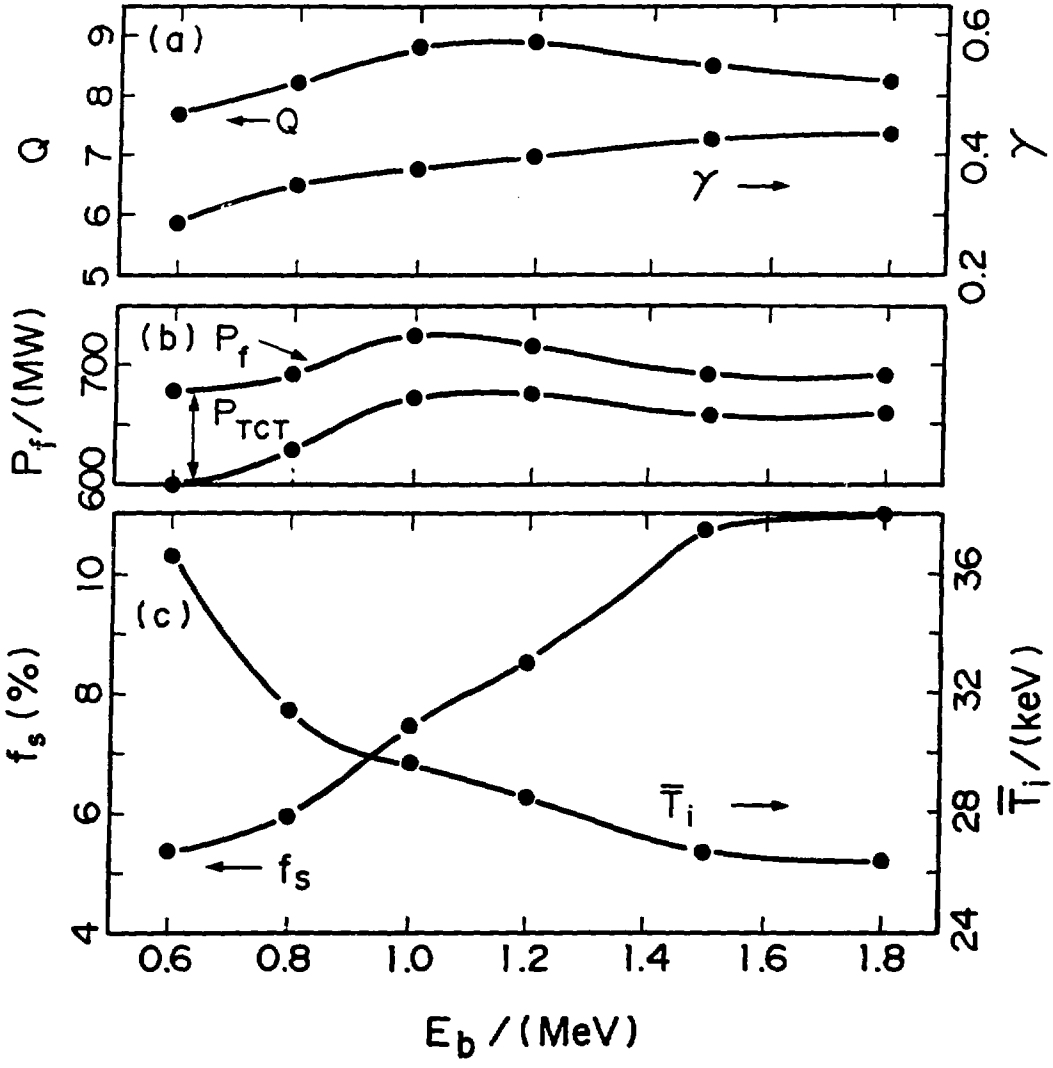

Fig. 8

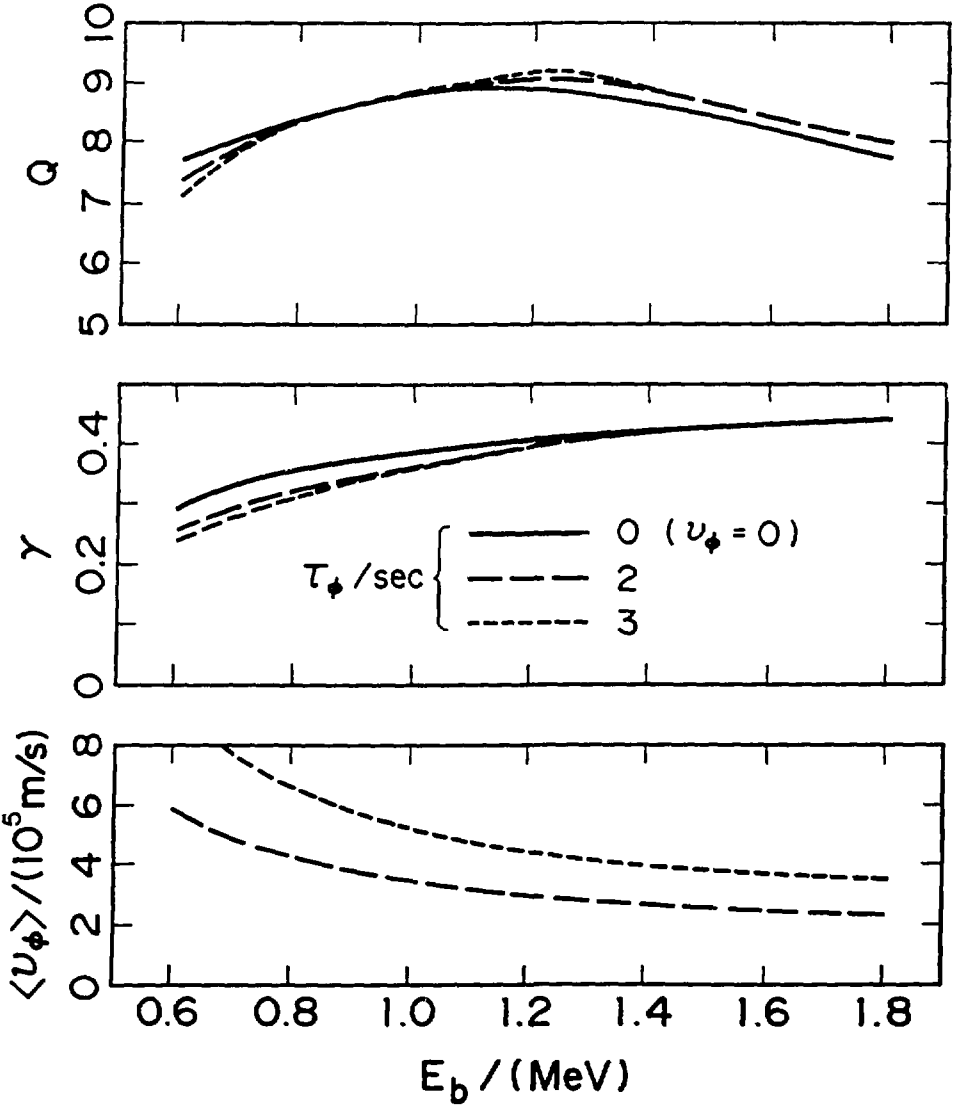
Q
5 6 7 8 9 10
γ
0 0.2 0.4
τφ /sec
0 (υφ = 0)
2
3
⟨υφ⟩/(10^5 m/s)
0 2 4 6 8
0.6 0.8 1.0 1.2 1.4 1.6 1.8
Eb / (MeV)

Fig. 9

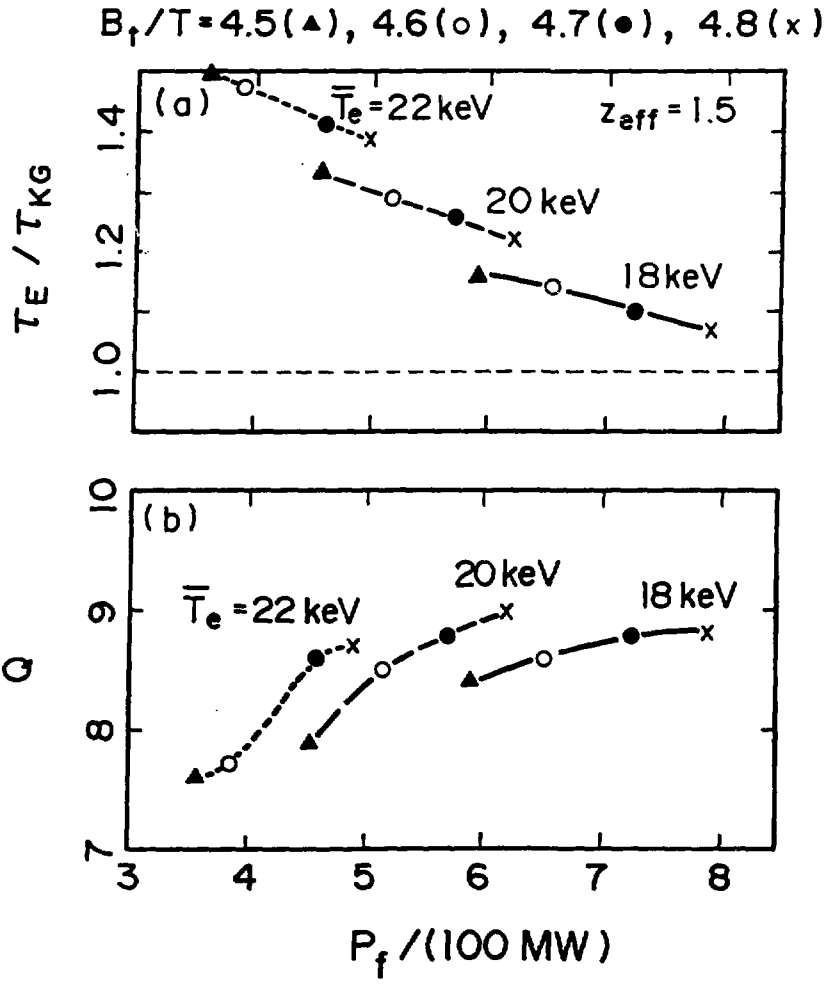
$B_t/T = 4.5(\blacktriangle), 4.6(\circ), 4.7(\bullet), 4.8(x)$
(a)
$\bar{T}_e = 22$ keV
$z_{eff} = 1.5$
20 keV
18 keV
τ_E / τ_{KG}
1.0
1.2
1.4
(b)
$\bar{T}_e = 22$ keV
20 keV
18 keV
Q
7
8
9
10
3
4
5
6
7
8
P_f /(100 MW)

Fig. 10